J Solid State Electrochem (2008) 12:1461–1467
DOI 10.1007/s10008-007-0489-8

ORIGINAL PAPER

Phase composition of electrodeposited silver-indium alloys

Ts. Dobrovolska · G. Beck · I. Krastev · A. Zielonka

Received: 25 September 2007 / Revised: 2 November 2007 / Accepted: 30 November 2007 / Published online: 11 January 2008

Abstract The phase composition of electrochemically obtained Ag-In alloy coatings electrodeposited at different conditions was determined. With the increase in the current density, both indium content and heterogeneity of the deposited layers increase. The amount of the indium-richer phase increase as well. Before the thermal treatment, the phases Ag, Ag_3In, and In_4Ag_9 are observed in coatings with spatio-temporal structures. As a result of heating the new phase Ag_4In appears at temperatures above 500 °C and indium is oxidized up to In_2O_3 from the oxygen in the heating chamber. Up to 500 °C, the spatio-temporal structures are still visible. Probably they consist of both Ag-rich α-phase and one of the phases of the alloy system with small indium content, such as Ag_4In or Ag_3In.

Keywords Electrodeposition · Phase composition · Self-organization phenomena · Silver-indium alloy

Introduction

Silver-indium alloy coatings have been enjoying close attention from today's industry for both their enhanced resistance to tarnishing in comparison to pure silver deposits [1, 2] and their excellent antifriction properties [3–5]. In a number of cases, they are obtained by vacuum technologies based on consecutive layer-by-layer coating of the separate metals and followed by a heat treatment [5]. The electrodeposition of the alloy is carried out mainly in alkaline cyanide electrolytes [1, 2, 6–11]. Silver in the cyanide complex is the more electropositive element in the system and the electrodeposition of the alloy is of a regular type according to A. Brenner [12]. Indium is present in the electrolyte as a mixed complex with the cyanide ions and the disintegration products of glucose, which is commonly used in the silver-indium electrolytes [10]. The difficulties arising from the instability of the alkaline electrolytes due to the low solubility of indium hydroxide [1, 13] are overcome by the electrolyte preparation procedure proposed in previous works [10, 14]. The obtained electrolytes are clear and stable and are able to be successfully used for the electrodeposition of the silver-indium alloy as well.

Silver is mainly deposited from the alloy electrolytes at low current densities. At higher current densities, silver deposits under a diffusion controlled conditions and the co-deposition of indium leads to formation of alloy coatings. With the increase in the indium content in the alloy, the silver lattice becomes gradually saturated with this element and a solid solution of indium in silver is formed. When the content of indium increases, the achieved excess leads to the formation of a new indium-richer phase. In this case interesting phenomena can be observed on the electrode surface, such as ordered spatial distribution of the different phases, due to the processes of self-organization and formation of spatio-temporal structures [2, 10, 11]. These coatings are phase-heterogeneous and consist of dark and light regions with different indium content [11]. Previous X-ray investigations show that in similar self-organized coatings the phases Ag, Ag_3In, In_4Ag_9, $AgIn_2$ and In can be established [11].

The phase composition of the Ag-In alloy system has been investigated by many authors [15–22]. The most cited work in the literature is that of Campbell et al. [20]. The

T. Dobrovolska (✉) · I. Krastev
"Rostislaw Kaischew" Inst. Phys. Chem. Bulg. Acad. Sci.,
1113 Sofia, Bulgaria
e-mail: tsvetina@ipc.bas.bg

G. Beck · A. Zielonka
Forschungsinstitut für Edelmetalle und Metallchemie,
73525 Schwäbisch Gmünd, Germany

denotations of the phases in the present paper are given according to the phase diagram in their work (Fig. 1) [20].

Hume -Rothery et al. [15] have determined the solubility limit of indium in silver. According to their investigations, at 315 °C the solubility limit of indium in silver is 21.7 wt %, but at room temperature it is 20.3 wt % [15]. According to other authors, this solubility limit is 20.4 wt % In [17]. According to thermoelectric measurements [22] the solubility limit of indium in silver should be approximately 2.1 at. %. These data sharply differ from the data of other investigations [15–21] and need to be confirmed by other methods of physico-chemical analysis. With the increase in the content of indium, the lattice parameter of the cubic α-phase (alpha) increase from 4.086 Å (at 0 wt % In) up to 4.149 Å (at 19.99 wt % In) [19].

The existence of the α′-phase (alpha_prime) is observed at indium contents in the alloy in the interval between 19.5 and 26.3 wt % [20]. According to Campbell et al. [20], α′ (alpha_prime) is the ordered form of the α-phase (alpha) where one indium atom occupies the corner position (0,0,0) of the cubic cell and the three silver atoms - the face-centred positions (0, 1/2,1/2) etc.

At indium contents between 25 and 100 wt %, the system is discussed in detail again in the work of Campbell et al. [20]. In this concentration interval the authors describe the presence of several phases as follows:

- β-phase: High temperature phase with a body-centred cubic lattice (phase transformation temperature between 660–695 °C) [19].
- γ-phase: Hexagonal phase (Ag_3In) with the range of homogeneity between 29 wt % and 29.7 wt % In at room temperature.
- ε-phase: Cubic phase, which corresponds to In_4Ag_9 (Ag_2In). The range of its homogeneity is between 32.8 wt % and 36.82 wt % In;
- φ-phase: Body-centred tetragonal phase, which exists together with the ε-phase from 36.8 wt % up to 67 wt % In, as well as with pure indium in the case of more than 67 wt % indium in the alloy. The phase corresponds to the $AgIn_2$ compound.

Silver is practically not soluble in indium.

In our previous investigations we established that the heterogeneous electrochemically obtained silver-indium alloy coatings consist of different phases, such as Ag, Ag_3In, In_4Ag_9, and $AgIn_2$ [11]. It has been established that in all investigated coatings with spatio-temporal structures on the cathode surface, the phases Ag, Ag_3In and In_4Ag_9 are observed. However, it is not possible to decode which of these phases exists in the dark areas of the coatings.

Other investigations on the phase composition of electrochemically deposited Ag-In alloy coatings are not known.

The aim of this study is to determine the phase composition of electrochemically obtained Ag-In alloy coatings electrodeposited at different conditions and to connect it with the observed changes in the spatio-temporal structures on the electrode surface.

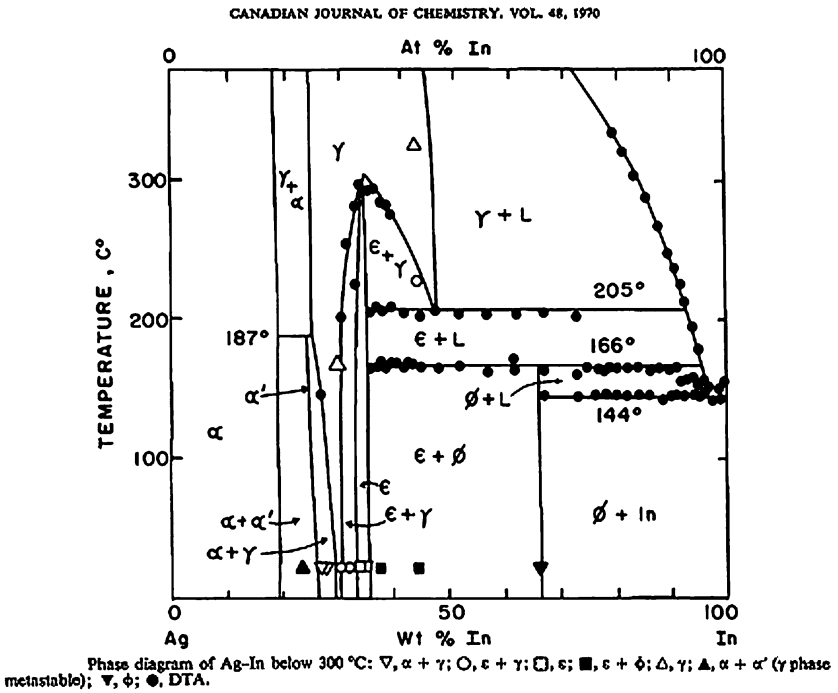

Fig. 1 Phase diagram of Ag-In system below 400 °C according Campbell et al. [20]

Materials and methods

The composition of the electrolyte for deposition of alloy coatings is given in Table 1.

The electrolytes were prepared using chemicals of *pro analisi* purity and distilled water by the following procedure: The necessary quantities of D(+)-Glucose were added to the water solution of indium chloride. The electrolyte was pre-electrolyzed for a short time while recording a cyclic voltammetric curve, or during galvanostatic deposition within 2–3 min with a current density of about 0.2–0.5 A.dm^{-2} in order to achieve some disintegration of the glucose [10] and after that the total amount of KCN according to the molar proportion of KCN to indium of 5:1 was added in one step to the electrolyte under stirring. After dissolution the silver salt was added.

The alloy coatings with thickness between 1 to 10 μm were deposited in the cell for cyclic voltammetric experiments under galvanostatic conditions. Copper and stainless steel cathodes with an area of 2×1 cm were used. The preliminary preparation of the copper cathodes includes a standard procedure of electrochemical degreasing followed by pickling in a 20% solution of sulphuric acid. In order to avoid the contact deposition of silver, the cathode was immersed into the electrolyte under current.

Two platinum counter electrodes (about 4 cm^2 each) were used. As a reference electrode an Ag|AgCl electrode ($Å_{Ag|AgCl}$=0.198 V vs. SHE) was used. The reference electrode was placed in a separate cell filled with 3 M KCl solution (Merck), connected to the electrolyte cell by a Haber-Luggin capillary through an electrolyte bridge containing also 3.M KCl solution. The experiments were carried out at room temperature by means of a computerized PAR 263A potentiostat/galvanostat using the software Soft Corr II.

The In percentage in the coatings depending on the electrodeposition conditions was determined by X-ray fluorescence analysis (Fischerscope X-RAY HDAL). The thickness and the percentage of the coatings were measured in 9 pointes - at 3 points in one row at the top, middle and low parts of the electrode.

By means of differential scanning calorimetry the temperatures of the probable phase transformations in Ag-In foils detached from the stainless steel substrates were established. The results were used to fix the temperature steps during the followed in situ X-ray investigations.

The X-ray patterns were measured in the 2θ range of 20 °–140 ° with the D8 Discover diffractometer (Bruker axs) in the Bragg-Brentano diffraction geometry. We used Cu-Kα radiation. The in situ measurements were performed at atmospheric conditions and at different temperatures (35, 150, 170 °C and in the range between 200 and 750 °C - in steps of 50 °C) within a heating chamber (DHS 900 Anton Paar). At each temperature one pattern was recorded 10 min and a second one 5 hr after reaching this temperature.

The elemental composition on the coating surface was measured by EDAX and the surface morphology was studied by SEM and optical microscopy.

Table 1 Composition of the electrolyte for deposition

Electrolyte composition	Concentration	
	g dm^{-3}	mol dm^{-3}
In as $InCl_3$ /Alfa Aesar/	22.4	0.2
Ag as $KAg(CN)_2$ /Degussa/	8	0.08
D(+)-Glucose / Fluka/	20	0.1
KCN /Merck/	65	1

Results and discussion

The surface characteristics of the galvanostatically deposited silver-indium alloy coatings onto copper substrates (electrolyte shown in Table 1) changes depending on the current density. The surface morphology was studied by optical microscopy, the indium content was established by X-ray fluorescence analysis, and the phase composition was determined by X-ray diffraction. Figure 2 shows a optical microscope image of the surface of a coating deposited at 0.1 A dm^{-2}. The coating is matt, homogeneous with the characteristic of silver's dull-white colour. The X-ray fluorescence analysis shows insignificant quantities of indium in the coatings (0.08 wt %). The X-ray pattern of this coating is presented on Fig. 3, curve A. Besides the strong silver reflections showing a preferred <111>-orientation, two other reflections of smaller intensity at 2Θ=36.5 ° and 2Θ=36.7 are registered. These reflections can be attributed neither to

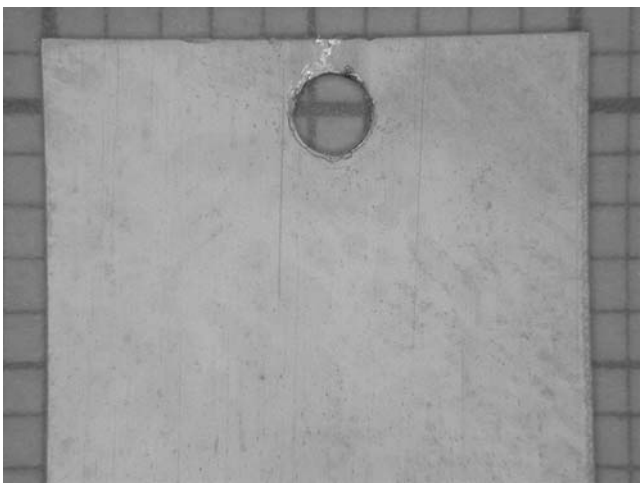

Fig. 2 Optical microscope image of the upper part of a coating deposited at 0.1 A dm-^{2} (electrode width – 1 cm, average In content less than 1 wt %)

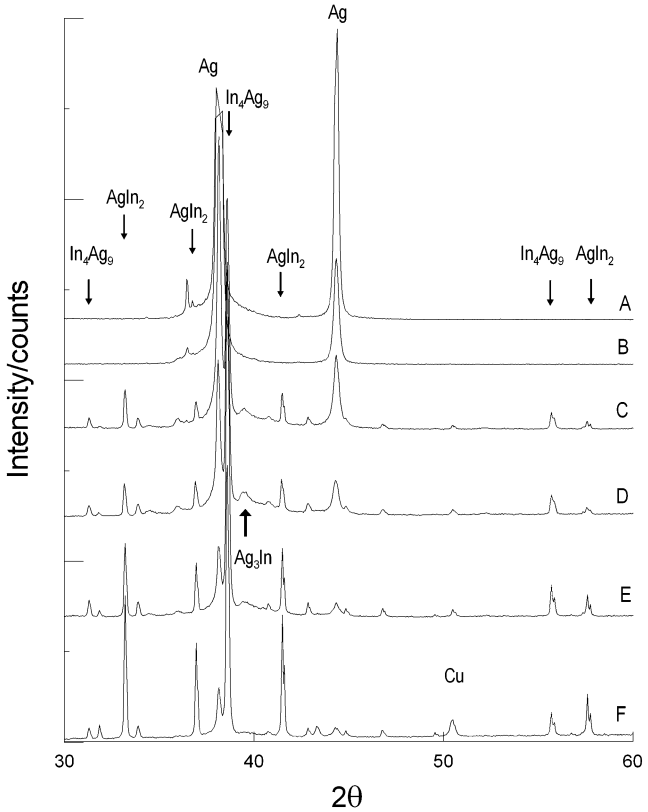

Fig. 3 Cut out of the X-ray patterns (in the 2Θ-region between 35° and 50°) of the coatings deposited at different current densities. **a** −0.1 A dm-^{2}; **b** −0.3 A dm-^{2}; **c** −0.5 A dm-^{2}; **d** −0.7 A dm-^{2}; **e** −0.9 A dm-^{2}; f −1.1 A dm-^{2}

the known silver-indium phases nor to the copper substrate. Their identification requires additional research.

The alloy coating deposited at 0.3 A dm^{-2} contains 0.14 wt % In. The microscopic studies show the same surface morphology of the coatings as in Fig. 2. The X-ray pattern (Fig. 3, curve B) is the same as that of the coating, deposited at 0.1 A dm^{-2}. Besides the reflections of silver with the preferred <111>-orientation, the reflections at the angles 2Θ=36.5° and 2Θ=36.7° are noted as well.

When increasing the current density up to 0.5 A dm^{-2} the coatings become heterogeneous (Fig. 4). The average contents of indium in the coating, measured by the X-ray fluorescence analysis, is 22.4 wt %. In this case the lowest measured percentage of indium could be found at the bottom part of the electrode reaching 1.1 wt % of indium, and the highest - in the upper part of the electrode reaching 44.4 wt %.

Besides the reflections of silver, very small reflections of the Ag_3In phase, as well as the reflections of the In_4Ag_9 and $AgIn_2$ phases can be found in the X-ray pattern of this coating (Fig. 3, curve C). A preferred orientation of the crystallites is not observed even for the silver.

The deposited coating at 0.7 A dm^{-2} is also heterogeneous, but more densely covered with dark areas. The

Fig. 4 Optical microscope image in the middle part of the surface of a coating; c.d. −0.5 Adm-^{2}; average In content 22.4 wt %; electrode width – 1 cm

average contents of indium in the coating is 26.4 wt %, with the lowest value of 11 wt % and the highest of 55 wt %. The phases In_4Ag_9 and $AgIn_2$ can be found in the X-ray pattern (Fig. 3, curve D) in addition to the silver phase (α-phase). Small reflections of the Ag_3In phase could also be registered. A preferred orientation of the crystallites in the coatings can not be registered at all.

At further increase in the current density up to 0.9 A dm^{-2} (average content of indium in the coating of 34.8 wt %, with the lowest value of 22 wt % and the highest of 53.8 wt %) and up to 1.1 A dm^{-2} (average content of indium in the coating of 44.3 wt %, with the lowest value of 42 wt % and the highest of 54.6 wt %), the coatings are still compact. However, they become even more heterogeneous (Fig. 5). The X-ray pattern of the coating deposited at 0.9 A dm^{-2} (Fig. 3, curve E) shows that the volume fraction of the

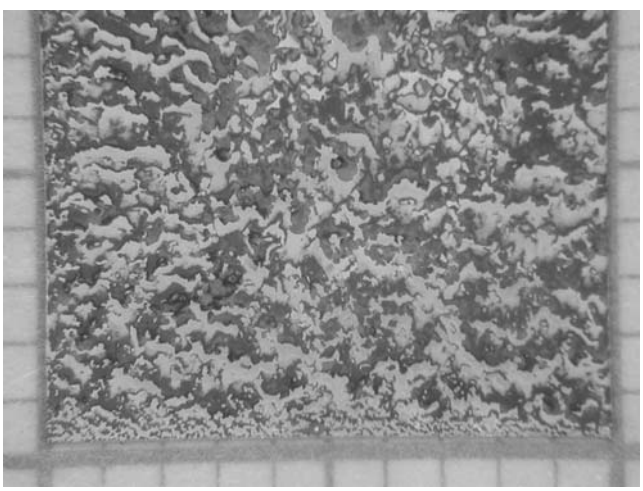

Fig. 5 Optical microscope image in the lower part of the surface of a coating; c.d − 0.9 A dm-^{2}; average In content 34 8 wt %; electrode width – 1 cm

silver phase continues to decrease and that of $AgIn_2$ phase increases compared to the In_4Ag_9 part.

Curve F (Fig. 3) shows the X-ray pattern of the coating deposited at 1.1 A dm^{-2}. Comparing this with the previous one (0.9 A dm^{-2}, Fig. 3 curve E), it can be seen that the volume fraction of the silver phase decreases again noticeably, but the volume fraction of the $AgIn_2$ phase increases significantly. Moreover, reflections of the copper substrate are registered, due to the diminishing of the thickness of the coating following the enforced co-deposition of indium [10, 11, 14].

The experimental results obtained during the investigation of the silver-indium alloy coatings depending on cathodic density allow us to draw the following conclusion: an X-ray diffraction analysis shows that the phases Ag_3In, In_4Ag_9, and $AgIn_2$ appear when the content of indium in the alloy is more than 22.4 wt%. As it could be expected, with the increase in the indium percentage in the alloy the amount of the indium-richer phase $AgIn_2$ increases.

Figure 6 summarizes the results about the established phase composition of the deposited coatings in dependence on the cathodic current density and the measured contents of both metals in the alloy. It is clear that due to the strong heterogeneity of the coatings most phases are registered together in one much broader concentration interval than this would correspond to a metallurgical obtained alloy with the same average content of indium. This is due to the fact that on one and the same electrode areas both of low and of high indium contents could be registered. An important conclusion of this study is that the phase Ag_3In appears, in spite of the small reflexes in the diffractogramms, in all samples, where spiral and other ordered structures are observed (Fig. 4).

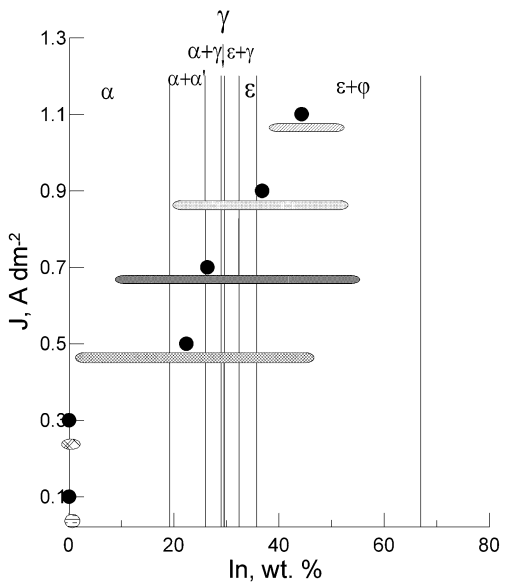

Fig. 6 Phase composition of the alloy coatings depending on the cathodic current density. Vertical lines - existence limits of the different phases after Campbel et al. [20]; horizontal bars - intervals of In percentage on different surface positions at the corresponding c.d.; ● - average In percentage of the whole sample

In many cases, such spatio-temporal structures are observed on the electrode surface [2, 11]. An attempt was made to solve the problem with the composition of the various dark and light areas by X-ray studies at high temperatures.

An Ag-In alloy coating, shown in Fig. 7, was deposited from the electrolyte (Table 1) onto a stainless steel substrate, and after detachment of the coating from the substrate the foil was subjected to DSC analysis. The results show that changes of the phase composition of the coating could be expected at temperatures about 168, 681 and 691 °C. This allows the determination of an appropriate sequence of temperature steps during the in situ X-ray measurements in the heating chamber.

Another coating, deposited onto a similar substrate under the same conditions (Fig. 8) was also investigated in the heating chamber by X-ray diffraction by stepwise increase in temperature.

Figure 9 shows all X-ray patterns of this temperature series. The comparison of measurements at the same temperature (after 10 min and after 5 hr) does not show significant differences. Characteristic positions of the peaks are marked with corresponding symbols. The reflexes due to the material of the heating chamber are marked as “H”.

The established phases on the different stages of the heat treatment are shown in Table 2.

With the increase in temperature, the number of available phases in the coatings decreases. At 150 °C, the phase In_4Ag_9 disappears and the appearance of a new phase Ag_4In is registered. This phase appears in the indium concentration range between the α-phase and the Ag_3In

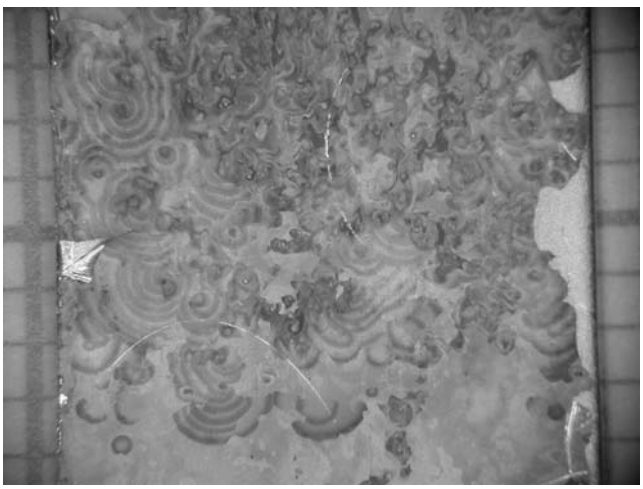

Fig. 7 Optical microscope image of a coatings surface before its detachment from the stainless steel substrate for DSC-measurement; c.d. − 0.15 A dm^{-2}; electrode width – 1 cm; average In content − 12.8 wt %

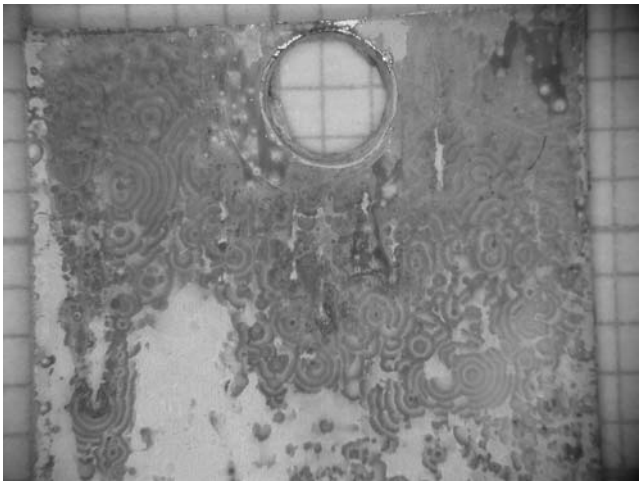

Fig. 8 Optical microscope image of a coatings surface before its detachment from the stainless steel substrate for X-ray measurement in the heating camera

phase. This probably results (as described by Straumanis et al. [21]) from the increase in the lattice parameter of the α-phase and the increase in the solubility of indium with the increase in temperature above 65 °C. At the average indium concentration of 12.8 wt % (the minimal, and the maximal values are 5.4 wt % and 20.2 wt %, respectively) the metallurgical alloy with the same content would be homogeneous. At higher temperatures, the hexagonal Ag_3In (250 °C) and the cubic Ag_4In (500 °C) phases disappear one after another. They are replaced by the cubic oxide phase of indium In_2O_3, i.e. with the increase of the temperature some separation of the alloy components can be reached.

The reflections position shift towards smaller 2Θ-angles during the increase in the temperature. This is due to the lattice expansion and the resulting increase in the lattice parameter. At temperatures above 500 °C the width of the lines profiles of the separate reflections in the patterns decreases. This suggests a significant enlargement of the

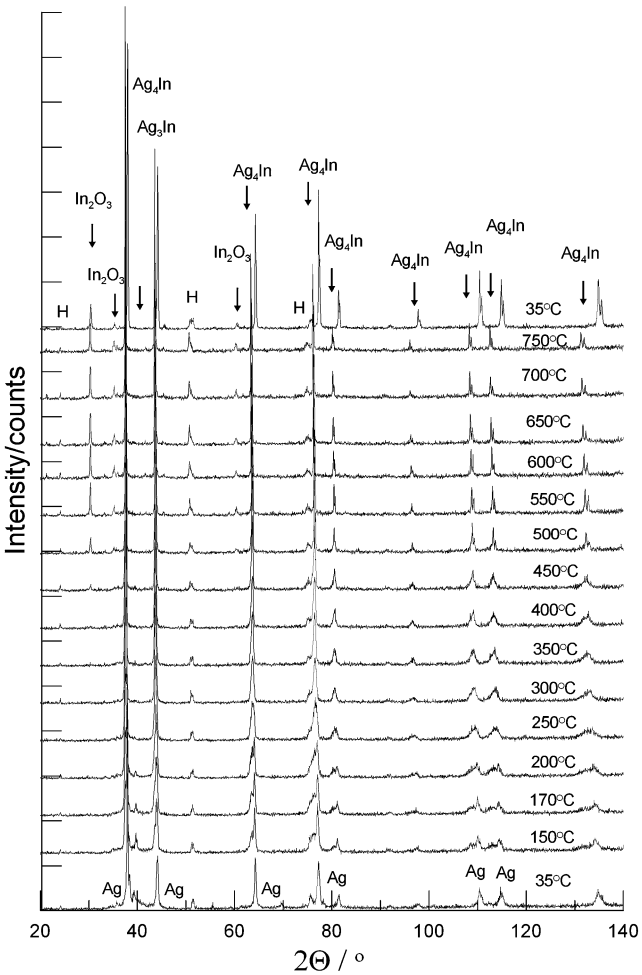

Fig. 9 X-ray patterns of the coating from Fig. 7 at different temperatures; 2Θ=20 up to 140 °

Table 2 Established phases on the different stages of the heat treatment

Stages of heat treatment	Established phases
35 °C (before heating)	Ag, cubic Ag_3In, hexagonal In_4Ag_9, cubic
150 °C (after 5 h)	Ag, cubic Ag_4In, cubic, formation Ag_3In, hexagonal (In_4Ag_9, cubic, disappearance)
250 °C (after 5 h)	Ag, cubic Ag_4In, cubic (Ag_3In, hexagonal, disappearance)
500 °C (after 5 h)	Ag, cubic (Ag_4In, cubic, disappearance) In_2O_3, cubic, formation
35 °C (after heating)	Ag, cubic In_2O_3, cubic

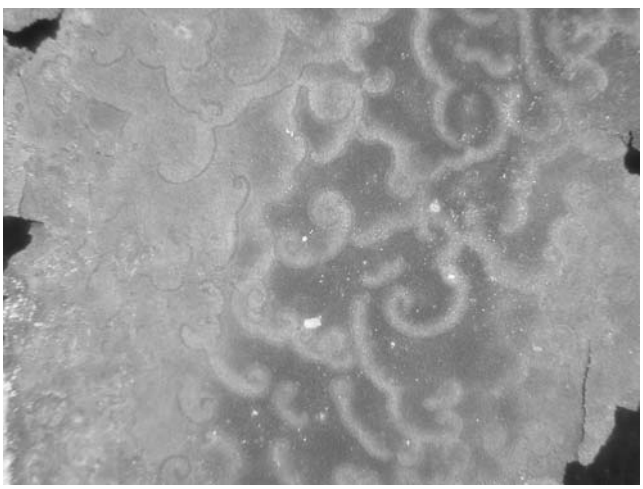

Fig. 10 Optical microscope image of a the coatings foil with periodic spatio-temporal structures after heating up to 500 °C and following cooling down to 35 °C; average In content 11 wt %, sample width-3 mm

crystallite size at temperatures higher than 500 °C. At similar temperatures In_2O_3 phase is formed and its volume fraction increases with increasing heating time.

Figure 10 shows that the spatio-temporal structures on the surface of the silver-indium foil can be seen well after a thermal treatment up to 500 °C. This means that they consist of phases able to remain stable at this temperature. The question remains whether the structures shown in Fig. 10 after the cooling down of the sample are the remains of some richer indium alloy phases such as Ag_3In or Ag_4In, respectively or one of them has appeared again at room temperature.

Conclusions

With the increase in the current density, both indium content and heterogeneity of the deposited layers increase. The amount of the indium-richer phase increase as well. The comparison of the results with the phase diagram according to Campbel et al. [20] shows the presence of all pertaining to the indium concentration range phases in the coating.

Before the thermal treatment, the phases Ag, Ag_3In, and In_4Ag_9 are observed in coatings with spatio-temporal structures. As a result of heating the new phase Ag_4In appears and at temperatures above 500 °C indium is oxidized up to In_2O_3 from the oxygen in the heating chamber.

Up to 500 °C, the spatio-temporal structures are still visible. Probably they consist of both Ag-rich α-phase and one of the next phases of the alloy system (according to the phase diagram) with small indium content, such as Ag_4In or Ag_3In.

Acknowledgments The authors are thankful to Deutsche Forschungsgemeinschaft (DFG) (Project 436 BUL 113/97/0-3) and to the FP6 European project NANOPHEN (INCO-CT-2005-106696) for supporting this study.

References

1. Gray D (1934) Trans Electrochem Soc 65:377
2. Raub E, Schall A (1938) Zeitschrift für Metallkunde 30:5149
3. US patent (1973) 1(389):192
4. US patent (1997) 5(684):847
5. US patent (1999) 5(879):819
6. Mohler JB (1945) Metal Finishing 43:60, 77
7. Walker R, Duncan SY (1982) Metal Finishing October:77
8. Viacheslavov PM, Grilihes SI, Burkat GK, Kruglova EG (1970) Galvanotechnika blagordnyh i redkih metallov. Mashinostroenie, Leningrad, p 202
9. Reksc W, Horoszkiewicz T (1986) Powloki Ochronne 79:12
10. Dobrovolska Ts, Krastev I, Zielonka A (2005) J Appl Electrochem 35:1245
11. Dobrovolska Ts, Veleva L, Krastev I, Zielonka A (2005) J Electrochem Soc 152:C137
12. Brenner A (1963) Electrodeposition of alloys, vol. I. Academic , New York, p 76
13. Goggin PL, McColm IJ, Shore R (1966) J Chem Soc A 10:1314
14. Dobrovolska Ts, Krastev I, Zielonka A (2004) Glavanotechnik 95:1134
15. Hume-Rothery W, Mabott GW, Evans KM (1934) Phil Trans Roy Soc A 233:1
16. Hume-Rothery W, Reynolds PW (1937) Proc Roy Soc A 160:282
17. Weibke F, Eggers H (1935) Z Anorg Chem 222:145
18. Owen EA, Roberts EW (1939) Phil Mag 27:294
19. Hansen M, Anderko K (1958) Constitution of binary alloys. McGraw-Hill, New York, p 26
20. Campbell AN, Wagemann R, Ferguson RB (1970) Canad J Chem 48:1703
21. Straumanis ME, Riad (1965) SM Trans Metallurg Soc AIME 233:964
22. Pollok DD (1967) Trans Metallurg Soc AIME 239:1768